International Journal of Lightweight Materials and Manufacture 3 (2020) 403–415

Contents lists available at ScienceDirect

International Journal of Lightweight Materials and Manufacture

journal homepage: https://www.sciencedirect.com/journal/international-journal-of-lightweight-materials-and-manufacture



Original Article

Modelling the effect of projectile hardness on the impact response of a woven carbon-fibre reinforced thermoplastic-matrix composite

Haibao Liu [a], Jun Liu [a], Yuzhe Ding [a], Jie Zheng [b], Lilong Luo [c], Xiangshao Kong [d], Jin Zhou [e], Bamber R.K. Blackman [a], Anthony J. Kinloch [a], John P. Dear [a, *]

[a] Department of Mechanical Engineering, Imperial College London, South Kensington, London, SW7 2AZ, United Kingdom
[b] AVIC The First Aircraft Institute, No. 1 East Renmin Road, Yanliang District, Xi'an, Shaanxi, 710089, People's Republic of China
[c] AVIC Aircraft Strength Research Institute, Xi'an, Shaanxi, 710065, People's Republic of China
[d] Department of Naval Architecture, Ocean and Structural Engineering, School of Transportation, Wuhan University of Technology, Wuhan, Hubei, 430063, People's Republic of China
[e] School of Mechanical Engineering, Xi'an Jiaotong University, Xi'an, 710049, People's Republic of China

ARTICLE INFO

Article history:
Received 5 March 2020
Received in revised form
20 May 2020
Accepted 26 May 2020
Available online 11 June 2020

Keywords:
Damage
Deformation
Impact
Numerical modelling
Projectile hardness
Thermoplastic composites

ABSTRACT

In the present paper numerical modelling results are described to predict the effects of the hardness of a projectile impacting a woven carbon-fibre reinforced thermoplastic-matrix composite. The projectiles are prepared from either relatively soft gelatine or hard high-density polyethylene (HDPE) materials, of the same mass, and are fired from a gas-gun at about 60 m s^{-1} to impact a woven carbon-fibre reinforced poly(ether-ether ketone) (woven CF/PEEK) composite. A two-dimensional, elastic, finite-element analysis (FEA) model is developed to simulate the gas-gun impact experiments and study the impact damage processes, and this numerical model is relatively computationally efficient. This FEA model makes predictions for the plastic flow for the gelatine projectile and the elastic deformation of the polyethylene projectile. In addition, the model predicts the effects of the hardness of the projectile on (a) the deformation of the impacted composite specimens and (b) the location and extent of damage in the composites. Very good agreement between the predictions from the model and the experimental measurements is observed. This research is of key importance in studying the behaviour of thermoplastic-matrix composites under impact loading by various types of threat such as relatively soft bodies, e.g. birds and hard objects, e.g. dropped-tools and runway debris.
© 2020 The Authors. Production and hosting by Elsevier B.V. on behalf of KeAi Communications Co., Ltd. This is an open access article under the CC BY-NC-ND license (http://creativecommons.org/licenses/by-nc-nd/4.0/).

1. Introduction

Fibre-reinforced polymer-matrix composite materials are finding widespread application in the transport industry and, in particular, in the commercial aircraft, rail and automotive sectors [1]. Based on an appropriate lay-up, composite laminates may possess very good in-plane properties, especially when these properties are normalised by the density of such composite laminates. However, laminated composites are very susceptible to some critical loading conditions, for example, through-thickness impact loading (e.g. Refs. [2–16]). Such loading can cause considerable damage, e.g. delamination, and a subsequent reduction in the strength and cyclic-fatigue properties in composite structures. This risk has significantly hindered the wider application of composite materials in primary load-carrying structures. Further, it has also been found that the responses of composites subjected to impact loading by projectiles with widely varying degrees of hardness may be very different [15]. A better understanding of the behaviour of composite laminates, subjected to impact loading by projectiles with very different degrees of hardness would greatly assist in the design and maintenance of composite aircraft structures. Since this aspect is of key importance in studying the behaviour of thermoplastic-matrix composites under impact loading by various types of threats such as relatively soft bodies, e.g. birds, and hard objects, e.g. dropped-tools and runway debris.

Now a recent paper [15] has reported detailed experimental measurements on using a gas-gun to fire relatively soft gelatine

* Corresponding author.
E-mail address: j.dear@imperial.ac.uk (J.P. Dear).
Peer review under responsibility of Editorial Board of International Journal of Lightweight Materials and Manufacture.

https://doi.org/10.1016/j.ijlmm.2020.05.005
2588-8404/© 2020 The Authors. Production and hosting by Elsevier B.V. on behalf of KeAi Communications Co., Ltd. This is an open access article under the CC BY-NC-ND license (http://creativecommons.org/licenses/by-nc-nd/4.0/).

projectiles or hard high-density polyethylene (HDPE) projectiles to impact woven carbon-fibre reinforced poly(ether-ether ketone) (woven CF/PEEK) composites. A Digital Image Correlation (DIC) system was used to record the deformation of the composite specimens during the impact event and a high-speed camera was also employed to record the behaviour of the projectiles. The results revealed that the composite specimens impacted by the hard HDPE projectiles underwent higher values of the out-of-plane (OOP) displacement than the composite specimens impacted by the soft gelatine projectiles. In addition, post-impact analyses demonstrated that the woven CF/PEEK composites were more vulnerable to damage when struck by the relatively hard HDPE projectile compared with the relatively soft gelatine projectile. The focus of the present paper is to attempt to quantitively model these previously reported [15] experimental measurements by developing a finite-element analysis (FEA) numerical model. The modelling results, including predictions of the response of the projectile as well as the deformation and resulting damage of the impacted composite specimen, are compared in detail with the experimental results.

2. Experimental studies

The experimental techniques used, and the results obtained, in the present paper have been previously reported [15]. Therefore, only a brief review is given here. A mixture of 10% by weight gelatine powder, supplied by Honeywell Specialty, Germany, and 90% by weight distilled water was employed to prepare the soft gelatine projectiles. HDPE rod, 'RS PRO Black' supplied by RS Components, UK, was used to manufacture the hard HDPE projectiles. The densities of the gelatine and HDPE projectiles were 1.06 ± 0.3% and 0.95 ± 0.2% g cm^{-3}, respectively; with hardness values of a Shore Hardness A of 5–10 and a Shore Hardness D of 60–70, respectively [15]. The gelatine and the HDPE projectiles had the same nominal diameter of 23 mm. To produce a similar mass, the HDPE projectiles had a nominal length of 50 mm, which was slightly longer than the 45 mm nominal length of the gelatine projectiles. Woven-T300 carbon-fibre reinforced PEEK composite prepregs, supplied by Haufler Composites, Germany, were used to manufacture the composite target specimens. The woven CF/PEEK prepregs were consolidated using an Out-of-Autoclave (OOA) manufacturing route. The lay-up and the nominal thickness of the woven CF/PEEK composite specimens were $[0^\circ{-}90^\circ]_{4s}$ and 2 mm, respectively.

A helium-propellant gas-gun was employed to launch the projectiles. A nominal impact velocity of 60 m s^{-1} was selected for this study as, at this velocity, it was possible to fire the projectiles reproducibly at the same velocity. (At a velocity lower than this, the projectile velocity varied and, at a higher velocity, the gelatine projectile would not maintain its shape.) A 3-D Digital Image Correlation (DIC) system, consisting of two high-speed cameras, was used to record the deformation of the composite specimen. A recording rate of 40,000 frames per second was employed for these two cameras. An area of study of 60 mm × 60 mm was defined for the DIC measurements. After the gas-gun impact experiments, a visual inspection was first performed of the tested composite specimens and, subsequently, a portable C-scan system was employed to undertake an ultrasonic scan in order to further investigate any damage suffered during the impact event.

3. Numerical modelling studies

3.1. Introduction

Fig. 1 shows the flow chart of the main FEA model which was implemented within the 'Abaqus/Explicit 2018' code. In the model, a time-stepping routine was implemented for every appropriate single element in the FEA model. The numerical model is stopped when the defined total time for the impact event has expired.

3.2. Modelling the response of the projectiles

In the present study, the Smoothed Particle Hydrodynamics (SPH) method [16,17] was adopted to analyse the deformation of the gelatine projectile. The SPH method employs the principle of Lagrangian mechanics, but in a meshless way. Such that, immediately after initial contact of the projectile with the composite, the solid FEA mesh for the gelatine impactor is substituted by interacting particle elements which are coupled by forces. In order to use the SPH method for capturing the response of the soft gelatine projectile, an equation of state (EOS), with suitable input parameters, is required for the modelling of the gelatine projectile. In the present research, the Mie-Grüneisen EOS, which is linear in energy, was employed to define the coupled equations [16,17]. To fit the Hugoniot pressure versus the nominal volumetric compressive strain curve, the linear U_s versus U_p relationship was employed as given by Ref. [16]:

$$U_s = c_0 + sU_p \tag{1}$$

where the fitting coefficient, s, is the slope of the linear relationship between U_s and U_p. The shock velocity in the gelatine projectile is U_s and the reference speed of sound is c_0. Considering the term U_p, the impact velocity of the projectile was assigned to be the value of U_p for all the 8-node linear-brick (C3D8R) elements when the model was started. When the simulation started, these elements for the projectile were converted to continuum particle (PC3D) elements and the value of U_p assigned to the particle elements was then continually updated based upon the loading conditions on the particles after the initial contact. The input parameters required for the numerical modelling of the gelatine projectiles are shown in Table 1 and are given in Ref. [18–20].

In the FEA model, the gelatine projectile is first represented by 8-node linear-brick (C3D8R) elements. When contact of the projectile occurs with the composite specimen, these linear-brick elements are then converted to continuum particle (PC3D) elements. In the present study, the PC3D elements were assigned a characteristic length of 0.5 mm. This characteristic length is half of the element size that is used for C3D8R elements which are employed initially to model the gelatine projectile. The masses chosen for the 8-node linear-brick (C3D8R) elements, or the continuum particle (PC3D) elements, were equally distributed because the projectile has uniform density and the total mass was equivalent. The hard HDPE projectile was simply modelled as an elastic material using C3D8R elements with a size of 1 mm × 1 mm × 1 mm.

3.3. Modelling the behaviour of the woven CF/PEEK composite

3.3.1. Introduction

For the modelling of the woven CF/PEEK composite specimen, the damage theories employed for this study have been discussed previously in Ref. [16]. These techniques were originally developed [21–24] for unidirectional fibre-reinforced composite plies and have been extended to cope with woven materials. This has been done for a $[0^\circ{-}90^\circ]$ woven carbon-fibre ply, which is incorporated into the woven CF/PEEK composite, by considering the system as two unidirectional-fibre sub-plies. These unidirectional sub-plies are then linked, perpendicular to the plane, of their fibre directions [16]. In the two-dimensional, elastic, FEA modelling, the sequence is to first create two unidirectional-fibre sub-plies. Each of these sub-plies has a thickness of the unidirectional-fibre sub-

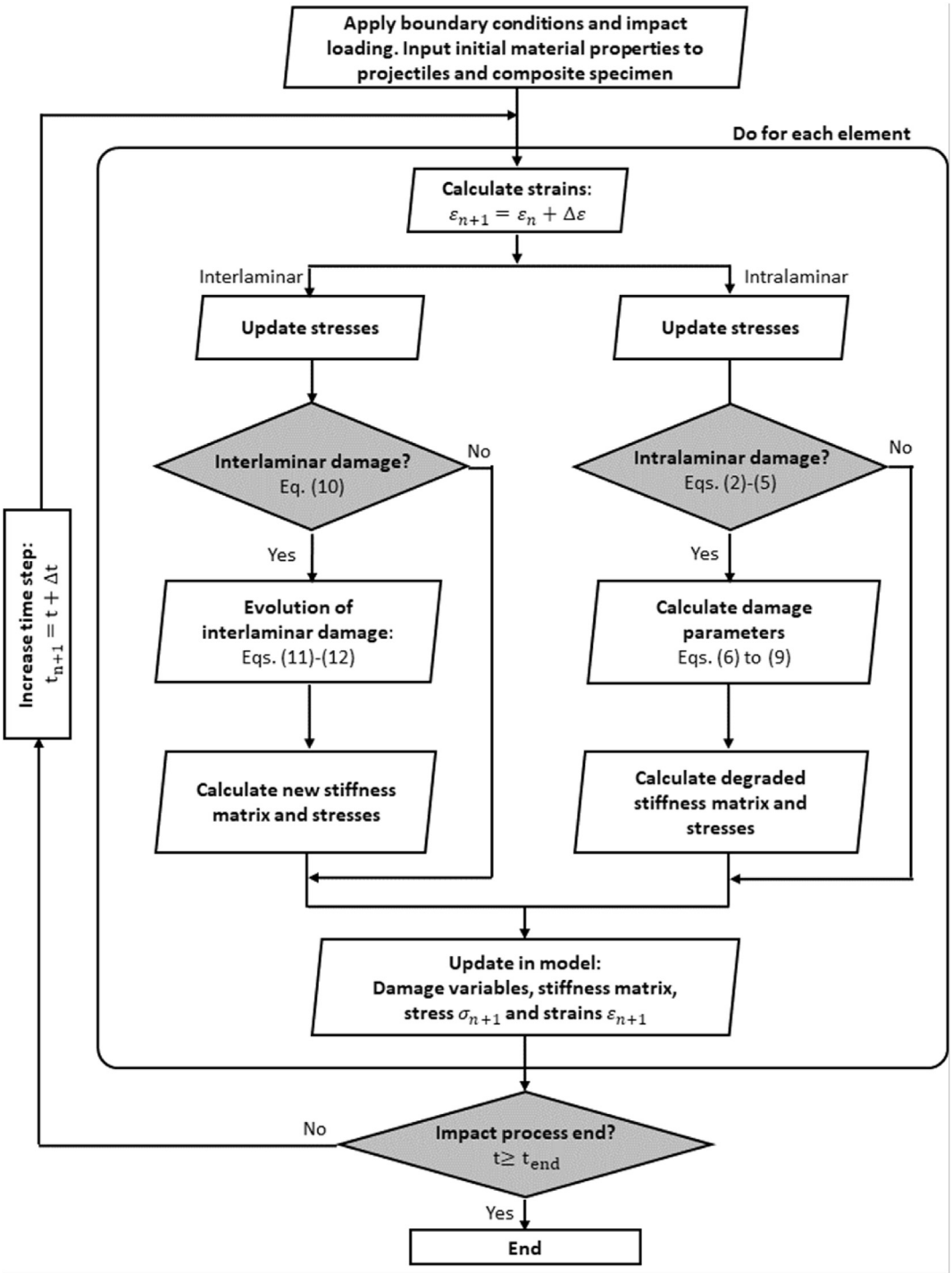


Fig. 1. The implementation of the two-dimensional FEA model showing schematically the flow chart, for one computation time-step, for a single element for modelling the interlaminar and intralaminar damage (The impact process typically runs from 0 to ca. 0.4 ms, with ca. 100 time-steps being employed in the FEA model.).

Table 1
Input parameters required for modelling the gelatine projectile [18–20].

Reference density	Dynamic viscosity	Reference speed of sound	Slope of the U_s versus U_p curve	Grüneisen ratio
1.06 g/ cm^3	1×10^{-6} MPa•s	$c_0 = 1.45 \times 10^6$ mm/s	$s = 1.87$	$\Gamma = 1.09$

ply of ca. 0.125 mm, which is equivalent to half of the thickness of the final equivalent [0°–90°] woven-fibre composite ply, which is ca. 0.25 mm. These two unidirectional-fibre sub-plies are then positioned at right angles to each other and are linked, out of their plane, using 'tie constraints', to form a single equivalent [0°–90°] woven-fibre composite ply. This has the same in-plane properties

as the actual woven-fibre composite ply that was used in the composite specimens. For the FEA modelling which followed, the elements employed for the composite target test specimens were 8-node quadrilateral in-plane general-purpose continuum shell (SC8R) elements, with an element size of 1 mm × 1 mm. The modelling results were found to be independent of the mesh size. The interfaces between the composite plies were modelled using a cohesive surface law, which is a built-in sub-routine within the 'Abaqus/Explicit 2018' code [16,21,24–26]. The boundary conditions employed in the model were the same as those used in the gas-gun experiments. A general contact algorithm was used to govern the global deformation at the contact interface, in the numerical modelling, and a friction coefficient of 0.2 was adopted for the global contact [27–29].

3.3.2. The intralaminar damage model

The initiation of intralaminar damage, in the modelling, was implemented within the 'Abaqus/Explicit 2018' FEA code, as described in a flow-chart, presented in Fig. 1. This approach was based upon Hashin's damage model for composites [21–23]. In this damage model, four different types of damage mechanism are identified. The damage mechanisms can be tensile fibre failure, compressive fibre failure, tensile matrix failure or compressive matrix failure, and each process is captured in the initiation of intralaminar damage, for each of the unidirectional-fibre sub-plies. A material coordinate system in the unidirectional-fibre sub-ply was defined as the 1–2–3 coordinate system, where the longitudinal fibre-direction is defined as the 11-direction and the transverse direction, perpendicular to the longitudinal fibre-direction, is defined as the 22-direction. Using this notation, it is possible to apply Hashin's damage approach, to model the initiation of the above four different types of damage as below:

$$\text{Tensile fibre failure}(\widehat{\sigma}_{11} \geq 0): \; F_f^t = \left(\frac{\widehat{\sigma}_{11}}{X^T}\right)^2 \tag{2}$$

$$\text{Compressive fibre failure}(\widehat{\sigma}_{11} < 0): \; F_f^c = \left(\frac{\widehat{\sigma}_{11}}{X^C}\right)^2 \tag{3}$$

$$\text{Tensile matrix failure}(\widehat{\sigma}_{22} \geq 0): \; F_m^t = \left(\frac{\widehat{\sigma}_{22}}{Y^T}\right)^2 \tag{4}$$

$$\text{Compressive matrix failure}(\widehat{\sigma}_{22} < 0); \quad F_m^c = \left(\frac{\widehat{\sigma}_{22}}{2S^T}\right)^2 + \left[\left(\frac{Y^C}{2S^T}\right)^2 - 1\right]\frac{\widehat{\sigma}_{22}}{Y^C} + \left(\frac{\widehat{\tau}_{12}}{S^L}\right)^2 \tag{5}$$

In the above equations, the indices on the terms F_f^t, F_f^c, F_m^t and F_m^c represent the different types of damage of tensile fibre failure, compressive fibre failure, tensile matrix failure and compressive matrix failure, respectively, and failure is predicted to occur when $F \geq 1$. The parameters, X^T and X^C denote the tensile and compressive strengths in the longitudinal fibre-direction, respectively. The terms Y^T and Y^C are the tensile and compressive strengths in the transverse direction, respectively; S^L and $S^T = Y^C/2$ denote the shear strengths in the longitudinal and transverse directions to the fibres, respectively; and the term $\widehat{\sigma}_{11}$, $\widehat{\sigma}_{22}$ and $\widehat{\tau}_{12}$ are components of the effective stress tensor, $\widehat{\sigma}$, that are used to evaluate the above criteria.

Corresponding to the damage initiation mechanisms defined in Hashin's criteria, four damage variables, d_f^t, d_f^c, d_m^t and d_m^c, were implemented in the damage evolution model. These damage variables have the value of 0 when the element is undamaged and 1 when fully damaged. A general form of the damage variable for a particular damage initiation mechanism is given by Ref. [21]:

$$d = \frac{\varepsilon^f(\varepsilon - \varepsilon^0)}{\varepsilon(\varepsilon^f - \varepsilon^0)} \tag{6}$$

where $d = d_f^t$ represents fibre tension failure, $d = d_f^c$ represents fibre compression failure, $d = d_m^t$ represents matrix tension failure and $d = d_m^c$ represents matrix compression failure, respectively. The strain, ε, is the equivalent strain in the composite ply. The strain values, ε^0 and ε^f, are the equivalent strains corresponding to the initiation of failure and final failure, respectively. For fibre tension or fibre compression failure, the terms ε, ε^0 and ε^f are assigned to be $\varepsilon = \varepsilon_{11}$, $\varepsilon^0 = \varepsilon_{11}^0$ and $\varepsilon^f = \varepsilon_{11}^f$, respectively. For tensile or compressive matrix failure, the terms ε, ε^0 and ε^f are assigned to be $\varepsilon = \varepsilon_{22}$, $\varepsilon^0 = \varepsilon_{22}^0$ and $\varepsilon^f = \varepsilon_{22}^f$, respectively. In the damage evolution model, the values of the initial failure strains, ε^0, are equal to the strain values corresponding to damage initiation, which may be directly obtained from the computation via implementing Equations (2)–(5), respectively. The final failure strains may be determined from a knowledge of the tensile, $G_{Ic}|_{ft}$, and compressive, $G_{Ic}|_{fc}$, intralaminar ply fracture energies in the longitudinal fibre-direction, and the tensile, $G_{Ic}|_{mt}$, and compressive, $G_{Ic}|_{mc}$, interlaminar ply fracture energies in the direction transverse to the fibre-direction [30].

Three damage parameters, d_f, d_m and d_s, which describe the extent of fibre damage, matrix damage and shear damage, respectively, were derived from the damage variables, d_f^t, d_f^c, d_m^t and d_m^c, as follows:

$$\text{For fibre damage: } \; d_f = \begin{cases} d_f^t, & \widehat{\sigma}_{11} \geq 0 \\ d_f^c, & \widehat{\sigma}_{11} < 0 \end{cases} \tag{7}$$

$$\text{For matrix damage: } \; d_m = \begin{cases} d_m^t, & \widehat{\sigma}_{22} \geq 0 \\ d_m^c, & \widehat{\sigma}_{22} < 0 \end{cases} \tag{8}$$

$$\text{For shear damage: } \; d_s = 1 - \left(1 - d_f^t\right)\left(1 - d_f^c\right)\left(1 - d_m^t\right)\left(1 - d_m^c\right) \tag{9}$$

During the evolution of damage, the derived damage parameters, d_f, d_m and d_s, were employed to degrade the stiffness matrix of the composite ply and to compute the degraded stresses that were acting. Further, when any of these three damage parameters exceeded the value of 0.99, then these damaged elements were deleted from the model. For more details, reference may be made to the Abaqus 2018 documentation [21].

3.3.3. The interlaminar damage model

To analyse the interlaminar damage, a quadratic-stress criterion was employed, which determines the initiation of any interlaminar damage in the composite laminates. This was implemented within the FEA code and the criterion is given by Ref. [16,21,31] as:

$$\left(\frac{\langle\sigma_n\rangle}{\sigma_n^0}\right)^2 + \left(\frac{\tau_s}{\tau_s^0}\right)^2 + \left(\frac{\tau_t}{\tau_t^0}\right)^2 = 1 \tag{10}$$

where σ_n represents the current stress acting normal to the ply, and τ_s and τ_t represent the current shear stresses acting on the ply. The values of the cohesive strengths, σ_n^0, τ_s^0 and τ_t^0 denote the interface tensile and shear strengths, respectively. Interlaminar damage is deemed to be initiated when the above quadratic interaction function attains, or exceeds, a value of one. Employing

the quadratic-stress criterion, it could be ascertained when the initiation of interlaminar damage occurred and the value of the displacement at the onset of damage initiation so deduced was termed δ^o.

The evolution of interlaminar damage during the impact event was modelled using a linear-softening material model embedded into a bilinear surface cohesive law [32], where the traction is plotted versus the displacement, δ. This was implemented as a subroutine in the FEA code [16,21,32]. This embedded interface element requires a value of the interlaminar fracture energy, G_c, and this term represents the area under the bilinear cohesive law. The energy-based Benzeggagh-Kenane (B–K) [33–35] criterion for Mixed-mode propagation was used to derive a value G_c for the growth of the delamination between the composite plies, as given by:

$$G_c = G_{Ic} + (G_{IIc} - G_{Ic})\left(\frac{G_{II}}{G_I + G_{II}}\right)^{\eta} \tag{11}$$

where G_{Ic} is the Mode I (opening tensile) interlaminar facture energy, G_{IIc} is the Mode II (in-plane shear) interlaminar facture energy and η is the B–K Mixed-mode interaction exponent, which may all be experimentally measured [33,35,36]. The parameters G_I and G_{II} are the current Mode I and Mode II energy-release rates, respectively, as calculated from the FEA code. Complete fracture of the interface element was assumed to occur, and hence delamination (i.e. interlaminar cracking) results, when the cohesive traction vanishes at the end of the degradation step. That is when the displacement, δ, of the interface element, as determined from the FEA code, attains the criterion:

$$\delta = \delta^f \tag{12}$$

where δ^f is the displacement of the interface element at failure, as fixed from a knowledge of the bilinear surface cohesive law. It should be noted that for the simulations of the location and extent of interlaminar damage that are deduced from the model then, following earlier work [25], a value corresponding to the displacement ratio of δ/δ^f of equal to, or greater, than 0.9 is used, i.e. to calculate the areas shown by the red colour in the figure shown later.

3.4. Input material properties

The input material properties for the gelatine projectile are given in Table 1 [18–20] and for the HDPE projectile the values of the density, tensile modulus and Poisson's ratio were taken to be 0.95 g cm^{-3}, 1.03 GPa and 0.45, respectively [37]. The input properties for the CF/PEEK composites are given in Table 2 [16].

4. Results and discussion

4.1. Behaviour of the projectiles

Fig. 2a shows the typical deformation history of the soft gelatine projectile, with an impact energy of 37 J which is associated with an impact velocity of 61 m s^{-1}, as obtained from the high-speed photographic images. The experimental results reveal that before contact with the composite specimen (i.e. time, $t = -0.3$ ms) the shapes of the gelatine projectile, and that of the HDPE projectile, were maintained during the flight of the projectiles. After the initial contact (i.e. $t = 0.0–0.1$ ms) the front of the gelatine projectile began to flow outwards. At a somewhat later stage (i.e. $t = 0.7$ ms) it was found that most of the gelatine projectile has spread over the composite specimen. These observations demonstrate that the gelatine projectile flowed freely after contact with the composite. In contrast, the sequence of images obtained from the impact of the HDPE projectile, for an impact energy of 34 J which is associated with an impact velocity of 58 m s^{-1}, are presented in Fig. 2b. It can be seen that no significant plastic or viscoelastic deformation occurred, which confirmed that the HDPE projectile underwent only elastic deformation during the impact event. For the HDPE projectile, the contact phase (i.e. $t = 0.0–0.4$ ms) is clearly evident and following this (i.e. at $t = 0.7$ ms) the HDPE projectile is clearly seen rebounding and so leaving the composite specimen. It is notable that for the gelatine projectile the whole impact event is much longer than that for the HDPE-projectile impact tests, with the gelatine projectile still flowing over the specimen at $t = 0.7$ ms, as is evident from Fig. 2.

To highlight the differences between the responses of the gelatine-impacted composites and the HDPE-impacted composites, the behaviour of the projectiles were modelled as a function of time for the 37 J gelatine-impacted composite and the 34 J HDPE-impacted composite, see Fig. 3a and b, respectively. (The legends in the figures indicate the values of the displacement in the projectile and of the out-of-plane (OOP) displacement, which are represented as the term U_3, with units of mm. The different colours in the legend represent different ranges for the predicted displacement.) When $t = 0$ ms, the colour of the projectile and composite are blue which reveals that all the U_3 displacements are zero. Once the projectile impacts the composite, there will now be a value for the corresponding displacement in the projectile and for the OOP displacement of the composite, as indicated by the corresponding colour in the legend. It can be observed that the HDPE projectile caused relatively more localised deformation in the woven CF/PEEK composite than the relatively soft gelatine projectile which is predicted to undergo extensive flow and deformation upon impact, as was indeed experimentally observed.

4.2. Deformation of the composites

The OOP displacement contours of the composite specimens subjected to the soft- and hard-impact loading were experimentally determined from the DIC results for the 37 J gelatine-impact and 34 J HDPE-impact events. The experimentally measured and numerically predicted OOP displacement contours are compared in Fig. 4 and very good agreement can be readily observed between the measured DIC values and the values predicted from the numerical modelling studies.

Fig. 5a presents the experimentally-measured and the numerically-simulated values of the central OOP displacements, with respect to the timescale of the impact event, with an energy level of 37 J for the gelatine-impacted and of 34 J for the HDPE-impacted woven CF/PEEK composites. Firstly, as may be seen, the experimentally measured and numerically predicted results are in very good agreement. Secondly, the HDPE-impacted composite shows a more rapid rise in the OOP displacement, and a higher maximum value, compared with the results for the gelatine-impacted composite specimen. Thirdly, for the HDPE-impacted composite, there is a plateau in the OOP displacement versus time response before the OOP displacement decays. This arises from the OOP plateau displacement being limited by the onset of fracture of the composite. It should be noted that during most of the time of the impact event (i.e. from about 0.05 ms to 0.3 ms) the central OOP displacement exhibited by the HDPE-impacted composite is higher than that for the gelatine-impacted composite, particularly for the latter part of the impact event (i.e. from about 0.2 ms to 0.3 ms). Also, of interest is that, for the gelatine impactor, the composite specimen has not returned to its initial position, by

Table 2
The input material properties for the CF/PEEK composite for the modelling studies [16].

Property	Unidirectional CF/PEEK sub-ply
Moduli (GPa)	$E_{11} = 127;\ E_{22} = 10.3;\ G_{12} = 5.7$
Poisson's ratio	$\nu_{12} = 0.3$
Strength values (MPa)	$X^T = 2070;\ Y^T = 85;\ X^C = 1360;\ Y^C = 276;$ $S^L = S^T = 186;$
Ply fracture energies (kJ.m^{-2})	$G_{Ic}\|_{ft} = 218;\ G_{Ic}\|_{fc} = 104;\ G_{Ic}\|_{mt} = 1.7;\ G_{Ic}\|_{mc} = 2.0$
Interlaminar fracture energies[a](kJ.m^{-2})	$G_{Ic} = 1.7\ ;\ G_{IIc} = 2.0$
B–K component[a]	$\eta = 1.09$
Cohesive strengths (MPa)	$\sigma_n^0 = 43;\ \tau_s^0 = \tau_t^0 = 50$
Initial cohesive stiffness (MPa.mm^{-1})	$k = 6.4 \times 10^5$

Notes:
G_{Ic} and G_{IIc} are the Mode I and Mode II interlaminar fracture energies between two [0°–90°] woven-fibre composite plies.
$G_{Ic}|_{ft}$ and $G_{Ic}|_{fc}$ are the tensile and compressive ply fracture energies of the unidirectional-fibre sub-plies in the longitudinal fibre-direction.
$G_{Ic}|_{mt}$ and $G_{Ic}|_{mc}$ are the tensile and compressive ply fracture energies of the unidirectional-fibre sub-plies in the transverse to fibre direction.
[a] These properties are for interlaminar failure between two of the [0°–90°] woven-fibre plies.

$t = 0.4$ ms, as the flow of the gelatine projectile is still causing deformation of the composite specimen.

Fig. 5b shows a comparison of the maximum central OOP displacements predicted using the FEA numerical model for the 37 J gelatine-impacted composite and the 34 J HDPE-impacted composite. The quantitative measurements and predictions of the maximum central OOP displacement that arise from employing the two different types of projectiles are shown and compared in Table 3. There is good agreement between the experimental and predicted values of the maximum central OOP displacement. Although, as may be seen, the SPH method is not as accurate in predicting this value. This is considered to be due the appreciable flow of the gelatine projectile that occurs and is a limitation of the SPH approach. The numerical predictions reveal that, when impacted by the gelatine projectile, the composite is predicted to undergo a maximum central OOP displacement of 3.7 mm. However, the CF/PEEK composite when impacted by the HDPE projectile is predicted to undergo a somewhat greater maximum OOP displacement of 4.1 mm, which is about 10% higher than when the soft gelatine projectile is used. Thus, the numerical modelling studies clearly reveal that the elastic HDPE projectile, with a relatively high hardness, is predicted to create a higher maximum value of the central OOP displacement in the composite compared to an impact by the soft gelatine projectile, when similar impact energy levels are employed.

4.3. Damage in the composites

Visual inspections and C-scanning examinations were undertaken on the impacted woven CF/PEEK composites, see Fig. 6 where three replicate composite specimens were tested. The visual inspection results, which are represented in Fig. 6 by the photographs taken of the rear-surface, indicated that the soft gelatine projectiles left no damage on the front- or rear-surfaces of the composite samples. The C-scanning images also show that no delamination is caused by the gelatine impact, see Fig. 6a where the C-scan results exhibit the extent of delamination with respect to the depth through the thickness of the composite specimen. (Here the red colour refers to the front (impacted) surface and the blue colour refers to the rear (non-impacted) surface of the tested specimens.) Photographs and C-scan images were also taken from the three HDPE-impacted CF/PEEK composite specimens, see Fig. 6b. The photographs reveal that all the HDPE-impacted specimens exhibit circular deformation patterns which are clearly visible on their rear-surfaces. Also, circular-shaped delaminations are observed from the C-scan images of the HDPE-impacted composite specimens. It is also noteworthy that these post-impact inspection images from the three replicate specimens for each type of projectile show that the gas-gun experiments delivered consistent results on undertaking the replicate tests.

To validate further the numerical model, the damage suffered by the woven CF/PEEK composite from both the experimental and the numerical studies for (a) the 37 J gelatine-impacted and (b) the 34 J HDPE-impacted specimens are compared in Fig. 7. (In this figure, the 'DAMAGESHR' legend for the modelling studies indicates the degree of intralaminar shear damage. This shear damage parameter has a range of 0–1, where the value of zero means that no damage has been initiated and the value of unity means complete damage has occurred, i.e. once the shear damage parameter of any element approaches the value of unity then no further shear damage can occur in the now fully-damaged element). As may be seen, in both cases for Fig. 7a and b there is a very good agreement between the experimental results and the numerical predictions. Indeed, it should be noted that the numerical studies have predicted very accurately the localised ring-pattern of damage that is experimentally observed on the 34 J HDPE-impacted composites, see Fig. 7b.

The high degree of accuracy observed in the numerical modelling studies may also be seen from a comparison of the delamination damage maps in the composites from the C-scanning experimental measurements and the FEA numerical predictions, as shown in Fig. 8. For the 37 J gelatine-impacted woven CF/PEEK composite, both the C-scan experimental results and the numerical predictions reveal that no interlaminar cracking occurs, see Fig. 8a. For the 34 J HDPE-impacted woven CF/PEEK composite, the predicted damage area is very similar in location and extent to that experimentally measured from the C-scan tests, see Fig. 8b. Thus, again, very good agreement is achieved between the experimental results and the numerical modelling predictions.

4.4. Impact failure mechanisms

In summary, from the above studies, comparing the results obtained from the composites impacted by the gelatine and HDPE projectiles, it was found that using the HDPE projectile resulted in (a) a larger maximum OOP displacement and (b) more impact-induced intralaminar damage and delamination in the woven CF/PEEK composite. To explain these phenomena, the deformation and failure mechanisms of the composite under a high-velocity impact by a soft gelatine projectile and hard HDPE projectile are illustrated

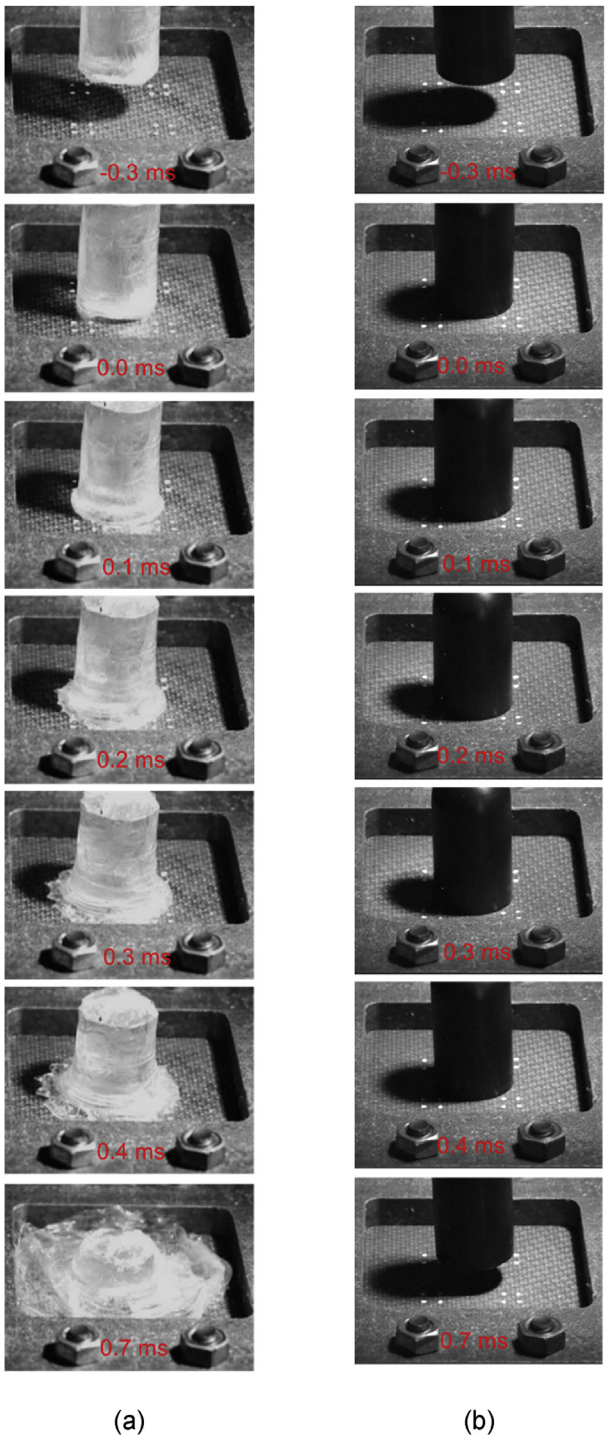


Fig. 2. The impact of the projectile against the woven CF/PEEK composite for: (a) the gelatine projectile striking with an impact velocity of 61 m s^{-1} and an impact energy of 37 J and (b) the HDPE projectile striking with an impact velocity of 58 m s^{-1} with an impact energy of 34 J. The time is given in ms, with 0.0 ms as the first point of contact. The gelatine and HDPE projectile both had a nominal diameter of 23 mm.

in the schematics shown in Fig. 9a and b, respectively. As soon as the projectile comes into contact with the front-surface of the composite specimen a shock wave is generated, associated with the initial high pressure (compressible) phase, see Fig. 9a–I. Soon after the initial contact, release waves form at the edges of the projectile, see Fig. 9a–II [38]. These release waves cause the formation of high-velocity flow, which travels with a relatively high transverse velocity across the impacted surface [39]. As shown in Fig. 9a–III, the generated shock wave would propagate along the axial direction of the projectile. Due to the flow of the gelatine, the gelatine projectile has a relatively large contact area on the impacted face of the composite, i.e. compare Fig. 9a–IV and b-IV. In contrast, for the impact by the HDPE projectile, after the initial contact, see Fig. 9b–I, shear stresses are generated within the composite via its contact with the external periphery of the hard HDPE projectile, as shown in Fig. 9b–II. This contact of the composite surface with the rounded edge of the relatively rigid HDPE projectile may then cause further damage in the composite specimen, see Fig. 9b–III. These effects lead to more localised damage in the composite on the rear-surface for an impact by the HDPE projectile, as may be seen from Fig. 9b–IV, compared with an impact by the gelatine projectile. Further, such damage on the rear-face of the composite surface is very likely to be visible in the form of a localised, circular, deformation pattern which mirrors the circular periphery of the hard HDPE projectile. Indeed, such damage was observed experimentally and was also captured by the numerical modelling studies, see Fig. 7b.

The duration of the high pressure (compressible) phase for the gelatine projectile, is determined by the time taken for the release wave to propagate from the outer edge of the gelatine projectile to the centre of the projectile [38]. On the other hand, the duration of the high pressure (contact) phase for the impact of the HDPE projectile is determined by the time taken for the shock wave to propagate along the length of the projectile, to the free end and then back to the impacted end. For the gelatine projectile impact, this gives the duration of the high-pressure phase as approximately $t = D/2U_s$ where D is the diameter of the projectile and U_s is the velocity of the release wave; and, assuming that it is equivalent to the shock velocity for the gelatine projectile, is 1560 m s^{-1}. This gives a duration of the high-pressure (compressible) phase of 0.007 ms. For the HDPE projectile, the contact time is given by $t = 2\ L/U_s$, where L is the length of the projectile and U_s is the shock velocity for the HDPE projectile. This gives a contact time of 0.04 ms, assuming a value of U_s for polyethylene of about 2400 m s^{-1}. These analytical predictions for the high pressure phase are in reasonable agreement with the results from the numerical modelling to be shown later. Now, the initial high-pressure phase for the gelatine-impacted composite is followed by a flow stagnation pressure phase as the gelatine flows across the impact surface. The consequence of this is that (a) the maximum out-of-plane (OOP) displacement for the gelatine projectile falls away more quickly after reaching a maximum and (b) the out-of-plane (OOP) displacement is greater for the HDPE-impacted composite, as shown in Fig. 5. Also, the gelatine-impacted composite is slower in returning to the undeformed position, as flow of the gelatine projectile is still occurring. However, the maximum OOP displacement occurs at nearly the same time-scale when using the gelatine- or the HDPE-projectile, since this is controlled by the dynamic (vibration) response of the clamped composite specimen when set into motion by the initial impact, and the mass of the projectile in contact with the specimen.

Now, the average contact pressure between the projectile and composite is simply defined by:

$$P_c = \frac{F}{A_c} \tag{13}$$

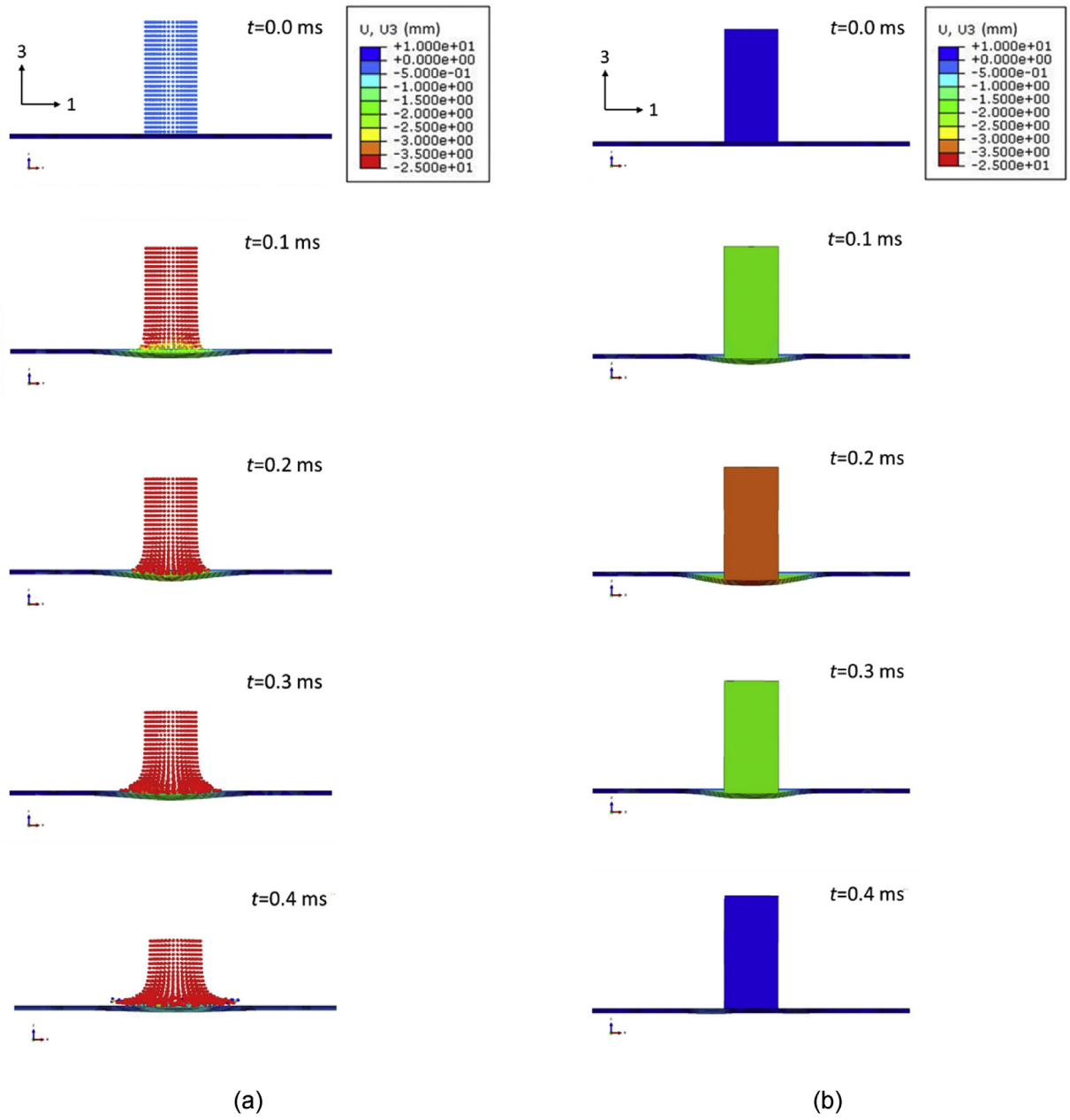


Fig. 3. The predicted out-of-plane (OOP) displacement of the composite specimen and the deformation suffered by the projectile modelled as a function of time for (a) the 37 J (i.e. an impact velocity of 61 m s^{-1}) gelatine-impacted woven CF/PEEK composite and (b) the 34 J (i.e. an impact velocity of 58 m s^{-1}) HDPE-impacted woven CF/PEEK composite. (The legends in the figures indicate the values of the displacement in the projectile and the OOP displacement of the composite specimen, which are represented as U_3, with units of mm. The different colours in the legend represent different ranges for the predicted displacement.)

where F is the impact load, and P_c and A_c are the average contact pressure and contact area between the projectile and the composite specimen, respectively. From the above discussions, there is a lower impact load and a higher contact area for the gelatine-impacted composite, compared with the HDPE-impacted composite. Therefore, the average contact pressure between the gelatine projectile and the composite will be lower, and hence the maximum central OOP displacement of the gelatine-impacted composite is again expected to be lower than that for the HDPE-impacted composite, as was found experimentally and predicted using the numerical model, see Fig. 5 and Table 3. Also, significantly less damage will therefore occur in the woven CF/PEEK composite when impacted by the gelatine projectile, again as found experimentally and predicted using the numerical model, see Figs. 7 and 8.

4.5. The contact pressure and loading of the composite by a soft- or hard-impact

To better understand the soft- and hard-impact behaviour of the composites, and also to confirm the above proposed impact mechanisms, the FEA numerical model was also employed to predict the average contact pressure between a projectile and the composite specimen, which could not be directly experimentally measured. The average contact pressure versus time history, as shown in Fig. 10a, was obtained from the numerical modelling simulations for (a) the woven CF/PEEK composite impacted by a gelatine projectile with an impact energy of 37 J, and (b) the woven CF/PEEK composite impacted by a HDPE projectile with an impact energy of 34 J. As may be seen, the HDPE-impacted woven CF/PEEK

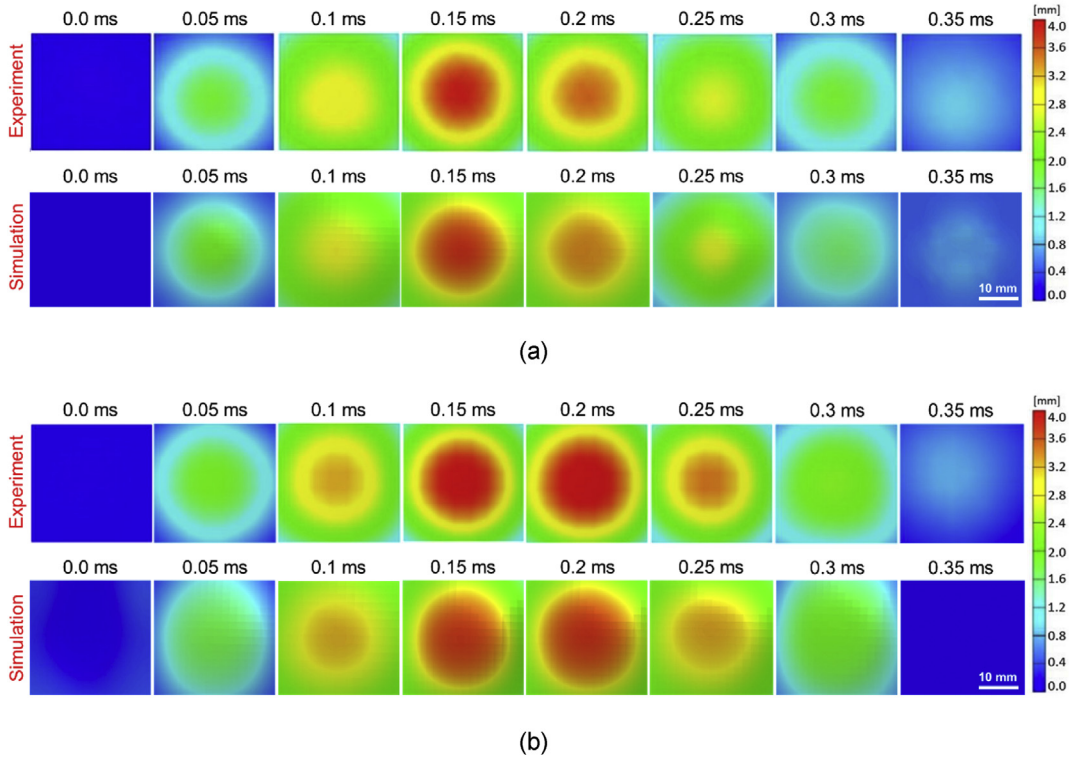


Fig. 4. The experimentally-measured and numerically-predicted OOP displacement contours of the woven CF/PEEK composite impacted by (a) a gelatine projectile with an impact energy of 37 J (i.e. an impact velocity of 61 m s^{-1}) and (b) a HDPE projectile with an impact energy of 34 J (i.e. an impact velocity of 58 m s^{-1}).

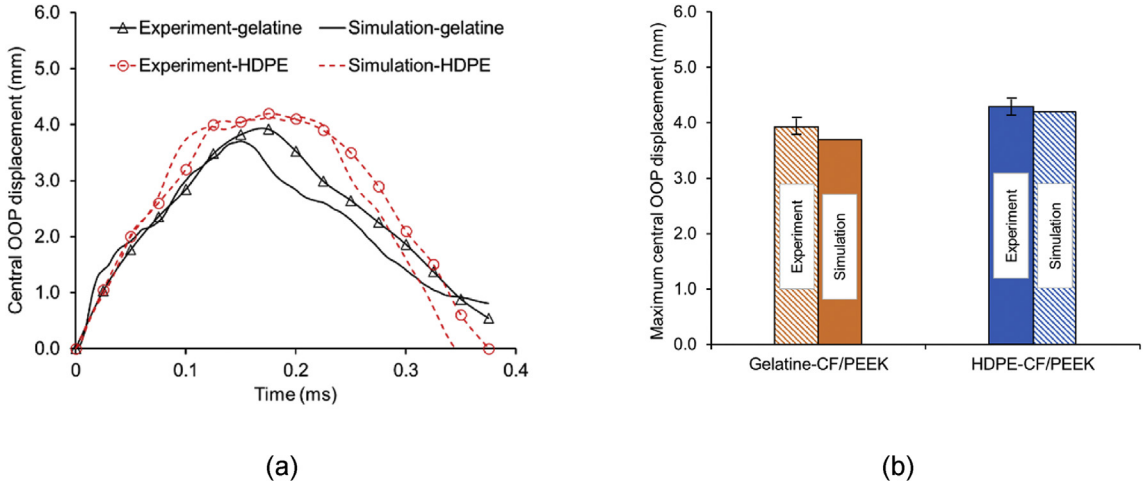


Fig. 5. The experimental and modelling simulation results for the woven CF/PEEK composite: (a) the central OOP displacement versus time trace and (b) the maximum OOP displacements for the 37 J gelatine-impacted (i.e. an impact velocity of 61 m s^{-1}) and the 34 J HDPE-impacted (i.e. an impact velocity of 58 m s^{-1}).

Table 3
Experimentally measured and numerically predicted maximum central OOP displacements in the impacted woven CF/PEEK composite.

Projectile	Energy level	Experiment (d_e)	Modelling (d_m)	Deviation $\left(\left\|\frac{d_m - d_e}{d_e}\right\| \times 100\%\right)$
Gelatine	37 J	3.9 mm	3.7 mm	5.1%
HDPE	34 J	4.2 mm	4.1 mm	2.4%

composite suffered a significantly higher average contact pressure. Indeed, the maximum average contact pressures for the gelatine-impacted and HDPE-impacted composites are 10.7 MPa and 29.3 MPa, respectively. For the soft impact by the gelatine projectile, after the initial high-pressure compressible phase, the gelatine flows over the composite specimen and the simulation shows an

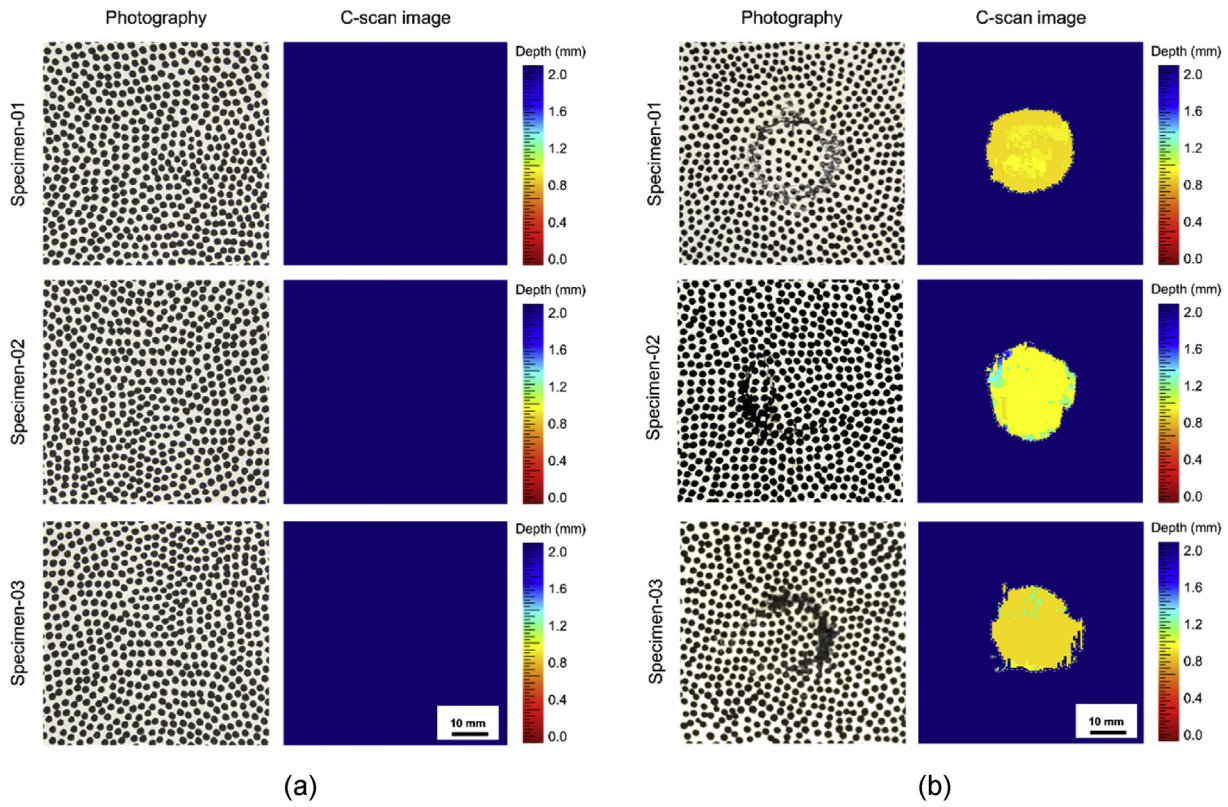


Fig. 6. Photographs of the rear-surfaces and the C-scan images of: (a) the woven CF/PEEK composite replicate specimens impacted by gelatine projectiles at an impact energy of 37 J (i.e. an impact velocity 61 m s^{-1}) and (b) the woven CF/PEEK composite replicate specimens impacted by HDPE projectiles at an impact energy of 34 J (i.e. an impact velocity 58 m s^{-1}). (The right-hand side scale for the experimental C-scan results indicates the location of the delamination as a function of the depth through the thickness of the specimen, where the red colour refers to the front (impacted) surface and the blue colour refers to the rear (non-impacted) surface of the composite specimen.).

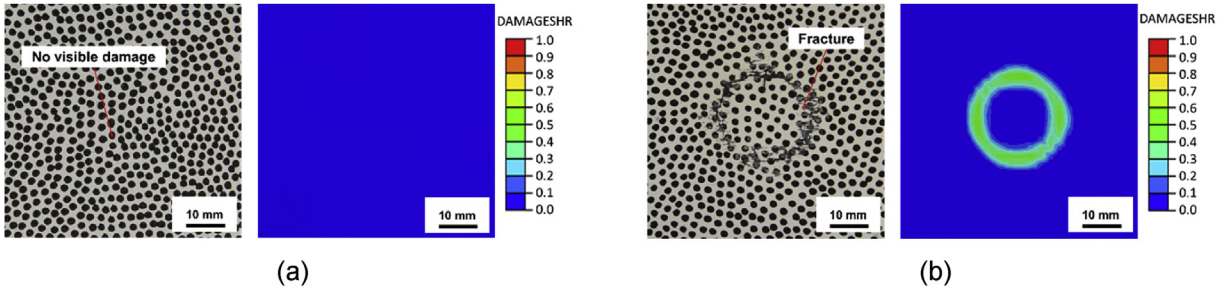


Fig. 7. Comparison of the damage in the rear-face of the composite specimens obtained from the experimental and the numerical modelling studies (a) the 37 J gelatine-impacted (i.e. an impact velocity 61 m s^{-1}): woven CF/PEEK composite and (b) the 34 J HDPE-impacted (i.e. an impact velocity 58 m s^{-1}) woven CF/PEEK composite. (The 'DAMAGESHR' legend for the modelling studies indicates the degree of intralaminar shear damage. This shear damage parameter has a range of 0–1, where the value of zero means that no damage has been initiated and the value of unity means complete damage has occurred, i.e. once the shear damage parameter of any element reaches the value of unity then no further shear damage can occur in the now fully-damaged element.)

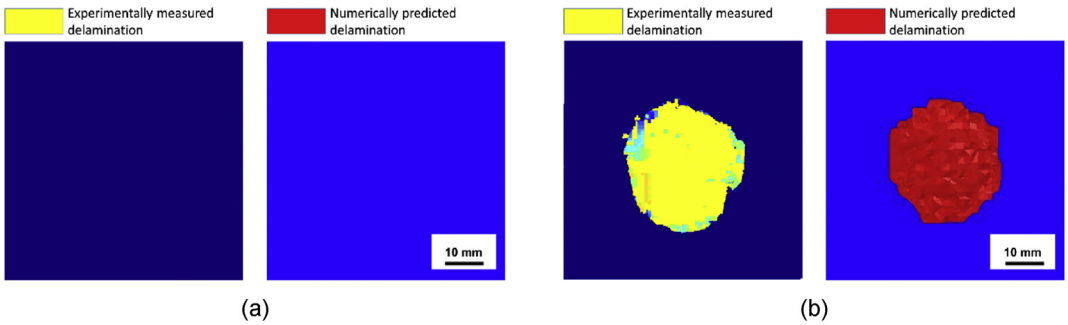


Fig. 8. Comparison of the location and extent of delamination in the composite specimens obtained from the experimental and the numerical modelling studies (a) the 37 J gelatine-impacted (i.e. an impact velocity 61 m s^{-1}): woven CF/PEEK composite and (b) the 34 J (i.e. an impact velocity 58 m s^{-1}) HDPE-impacted woven CF/PEEK composite.

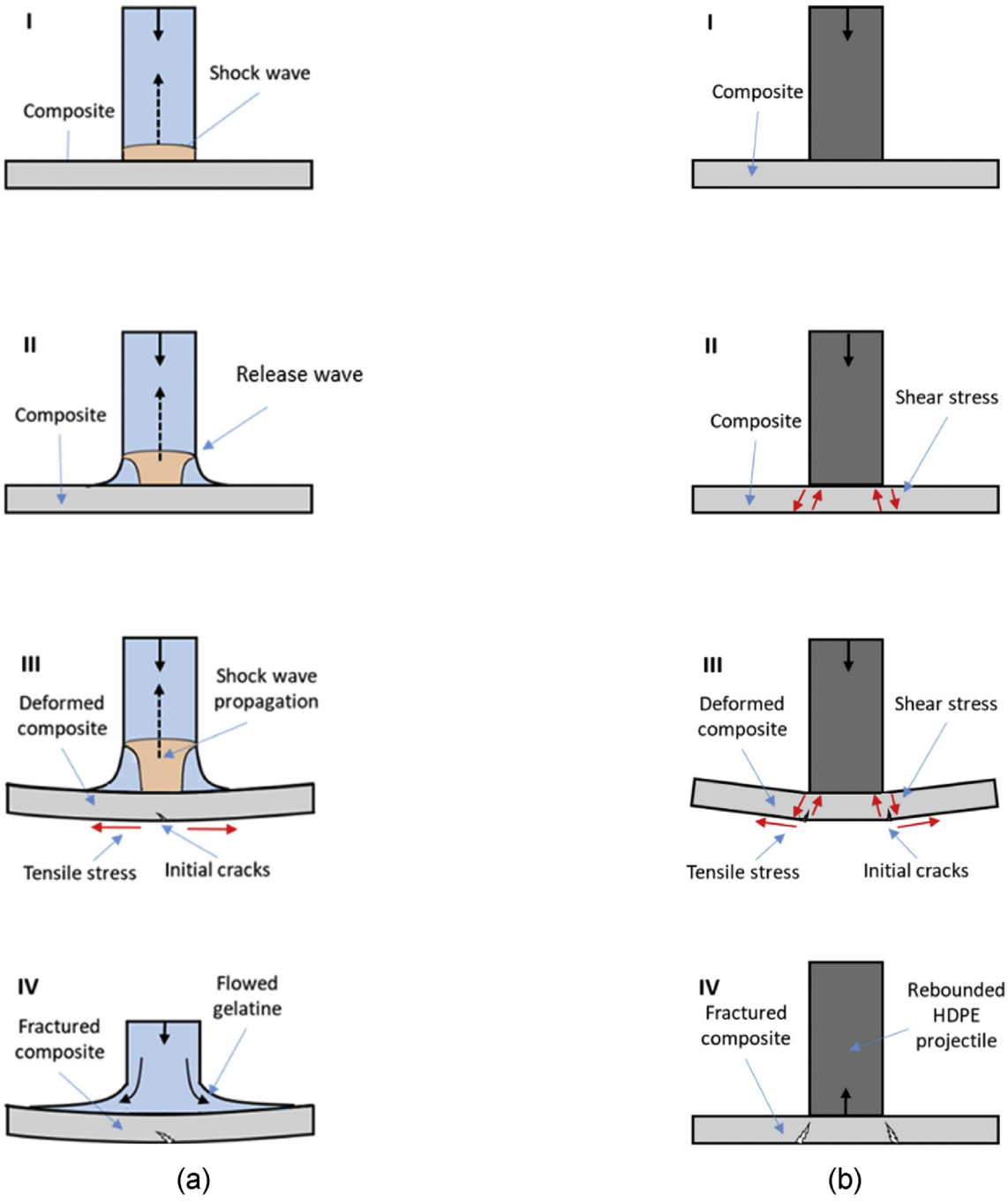


Fig. 9. Schematics of the impact test for different types of projectile: (a) a specimen impacted by the soft gelatine projectile and (b) a specimen impacted by the hard HDPE projectile.

average contact pressure of about 2 MPa. This is consistent with the stagnation pressure associated with incompressible flow of a liquid at about 60 m s^{-1}, i.e. the pressure, $P = 1/2\ \rho U_p{}^2$, where ρ is the density of gelatine, and hence $P = 1.9$ MPa.

Fig. 10b shows the predicted load versus time curves obtained from simulations of both the soft- and hard-projectile impacting the composite specimen. The results show that the maximum load for the gelatine-impacted and HDPE-impacted composites were 4.2 kN and 12.5 kN, respectively. However, it should be noted that the gelatine projectile is still exerting a load beyond 0.4 ms. An interesting point is that the impulse associated with the HDPE impactor is about 1.5 N s, i.e. an average load of 5 kN for 0.3 ms, which will bring about a change in momentum of the incoming HDPE projectile of about 1.5 kg m s^{-1}. Now, the initial incoming momentum of the HDPE projectile is 1.1 kg m s^{-1}, so this indicates that the projectile will rebound with a momentum of about 0.4 kg m s^{-1}, which is consistent with the observation that the rebound velocity was about 20 m s^{-1}.

It is more difficult to relate the area under the pressure versus time curve for the gelatine-impacted composite to the total incoming momentum of the projectile. After the initial compressible phase, which sets the specimen in motion, the SPH simulation of the interacting particles, which represent this soft impactor, are deflected by the composite specimen impactor. At $t = 0.4$ ms, the

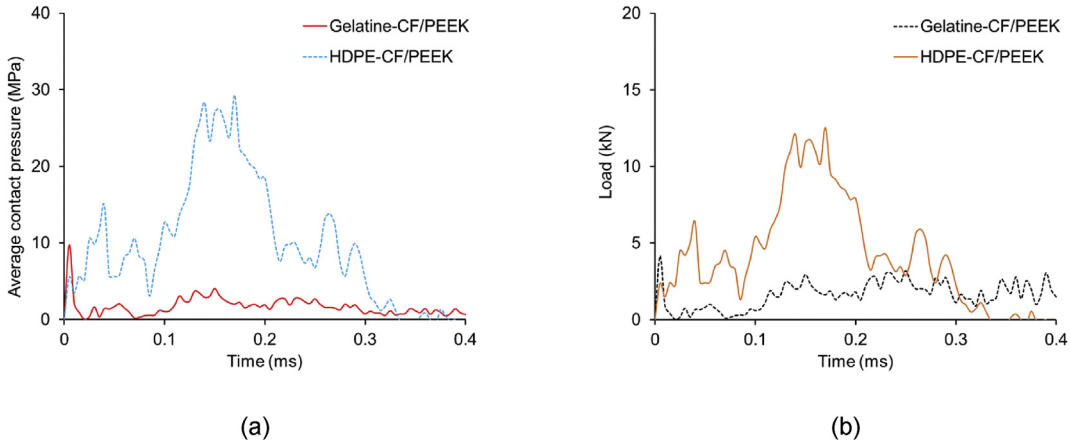


Fig. 10. Predictions from the numerical model for: (a) the average contact pressure versus time history and (b) the load versus time history. For the woven CF/PEEK composite impacted by the gelatine projectile with an impact energy of 37 J (i.e. an impact velocity 61 m s^{-1}) or impacted by the HDPE projectile with an impact energy of 34 J (i.e. an impact velocity 58 m s^{-1}).

gelatine projectile is still impacting the specimen. On the other hand, the HDPE projectile is brought to rest, deforms elastically and then rebounds within 0.4 ms. The consequence of this is that the impact event for the HDPE projectile is well defined, but the impact event for the gelatine projectile is much longer, as evident in Figs. 4, 5 and 10. (Note that the maximum OOP displacement occurs at about $t = 0.2$ ms when using the gelatine projectile or the HDPE projectile, as this is controlled by the dynamic (vibration) response of the clamped composite specimen when set into motion by the initial impact, and the mass of the projectile in contact with the specimen.)

These predicted values reveal that the elastic HDPE projectile, with a relatively high hardness, gives a significantly higher contact pressure when impacting the composite specimen. This clearly confirms the mechanisms given above for why significantly greater displacements and damage are suffered by the HDPE-impacted composite, compared with the gelatine-impacted composite.

5. Conclusions

This paper has presented a numerical modelling study on the effects of the hardness of the projectile on the impact behaviour of a woven carbon-fibre reinforced poly (ether-ether ketone) (woven CF/PEEK) composite. The projectiles were prepared from either relatively soft gelatine or hard high-density polyethylene (HDPE) materials, of the same mass, and were fired from a gas-gun at about 60 m s^{-1} to impact the composite.

A two-dimensional, elastic, finite element analysis (FEA) model has been developed to predict the behaviour of the composites under impact loading by these projectiles, which possess very different values of hardness. This two-dimensional, elastic, FEA numerical model is relatively computationally efficient and various sub-models have been integrated within this FEA model. For example, these include (a) a smooth particle hydrodynamics (SPH) model to simulate the viscoelastic/plastic flow of the gelatine projectile or an elastic model for the hard high-density polyethylene (HDPE) projectile, (b) the Hashin damage model and a quadratic-stress criterion for predicting the initiation of intralaminar or interlaminar damage, respectively, in the composite and (c) a damage variable approach and a bilinear softening law for modelling the evolution of any intralaminar or interlaminar damage, respectively, in the composite. The results from the modelling predictions were in very good agreement with the experimental results and showed that the effects of projectile hardness can be quantitatively modelled with regards to predictions of: (a) the response of the projectile, (b) the deformation of the impacted composite specimens and (c) the location and extent of damage suffered by the composite. Indeed, both the experimental and numerical results showed that the woven CF/PEEK composite suffered a higher out-of-plane (OOP) displacement and more impact-induced damage when impacted by the relatively hard HDPE projectile than by the soft gelatine projectile. Mechanisms for these observations have been proposed and validated from the FEA numerical studies.

The present research is of direct relevance to the commercial aircraft industry, since carbon-fibre composites based upon thermoplastic matrices are finding increasing applications and can experience damage from relatively soft bodies, e.g. birds, and as well as harder objects, e.g. dropped-tools and runway debris.

Conflicts of interest

The authors declare that there is no conflicts of interest.

Acknowledgements

The strong support from the Aviation Industry Corporation of China (AVIC) Manufacturing Technology Institute (MTI), the First Aircraft Institute (FAI) and the Aircraft Strength Research Institute (ASRI) for this funded research is much appreciated. The research was performed at the AVIC Centre for Structural Design and Manufacture at Imperial College London, UK.

References

[1] B. Krishan, K.K. Chawla, Composite Materials: Science and Engineering, Springer Science & Business Media. Springer-Verlag New York, USA, 2012.
[2] K. Stellbrink, On the behaviour of impact damaged CFRP laminates, Fibre Sci. Technol. 18 (1983) 81–94.
[3] M.N. Ghasemi Nejhad, A. Parvizi-Majidi, Impact behaviour and damage tolerance of woven carbon-fibre reinforced thermoplastic composites, Compos 21 (1990) 155–168.
[4] W.J. Cantwell, J. Morton, The impact resistance of composite materials – a review, Compos 22 (1991) 347–362.
[5] C. Soutis, P.T. Curtis, Prediction of the post-impact compressive strength of CFRP laminated composites, Compos. Sci. Technol. 56 (1996) 677–684.
[6] J.K. Kim, M.L. Sham, Impact and delamination failure of woven-fabric composites, Compos. Sci. Technol. 60 (2000) 745–761.
[7] E. Selver, P. Potluri, P. Hogg, C. Soutis, Impact damage tolerance of thermoset composites reinforced with hybrid commingled yarns, Compos Part B 91 (2016) 522–538.

[8] G. Balaganesan, V.C. Chandra, Energy absorption of repaired composite laminates subjected to impact loading, Compos. B Eng. 98 (2016) 39–48.
[9] M. Ravandi, W.S. Teo, L.Q.N. Tran, M.S. Yong, T.E. Tay, Low velocity impact performance of stitched flax/epoxy composite laminates, Compos Part B 117 (2017) 89–100.
[10] P. Turner, T. Liu, X. Zeng, K. Brown, Three-dimensional woven carbon fibre polymer composite beams and plates under ballistic impact, Compos. Struct. 185 (2018) 483–495.
[11] H. Liu, B.G. Falzon, W. Tan, Experimental and numerical studies on the impact response of damage-tolerant hybrid unidirectional/woven carbon-fibre reinforced composite laminates, Compos. B Eng. 136 (2018) 101–118.
[12] R. Mohamadipoor, M.H. Pol, E. Zamani, Nonlinear analytical study of thin laminated composite plate reinforced by nanoparticles under high-velocity impact, Thin-Walled Struct. 127 (2018) 446–458.
[13] H. Jiang, Y. Ren, Z. Liu, Numerical prediction for effects of fiber orientation on perforation resistance behaviors of patch-repaired composite panel subjected to projectile impact, Thin-Walled Struct. 144 (2019) 106325.
[14] H. Tan, L. Liu, Y. Guan, W. Chen, Z. Zhao, Investigation of three-dimensional braided composites subjected to steel projectile impact: experimental study and numerical simulation, Thin-Walled Struct. 140 (2019) 144–156.
[15] H. Liu, J. Liu, C. Kaboglu, H. Chai, X. Kong, B.R.K. Blackman, A.J. Kinloch, J.P. Dear, Experimental investigations on the effects of projectile hardness on the impact response of fibre reinforced composite laminates, Int. J. Lightweight Mater. Manuf. 3 (2020) 77–87.
[16] H. Liu, J. Liu, C. Kaboglu, J. Zhou, X. Kong, B.R.K. Blackman, A.J. Kinloch, J.P. Dear, The behaviour of fibre-reinforced composites subjected to a soft impact loading: an experimental and numerical study, Eng. Fail. Anal. 111 (2020) 101448.
[17] A.F. Johnson, M. Holzapfel, Modelling soft body impact on composite structures, Compos. Struct. 61 (2003) 103–113.
[18] H. Frissane, L. Taddei, N. Lebaal, S. Roth, SPH modeling of high velocity impact into ballistic gelatin. Development of an axis-symmetrical formulation, Mech. Adv. Mater. Struct. 3 (2018) 1–8.
[19] S. Abdul Kalam, R. Vijaya Kumar, G. Ranga Janardhana, SPH high velocity impact analysis-influence of bird shape on rigid flat plate, Mater. Today Proc. 4 (2017) 2564–2572.
[20] S. Georgiadis, A.J. Gunnion, R.S. Thomson, B.K. Cartwright, Bird-strike simulation for certification of the Boeing 787 composite moveable trailing edge, Compos. Struct. 86 (2008) 258–268.
[21] Abaqus 2018 Documentation, Dassault Systèmes, Provid, Rhode Island, USA, 2018.
[22] Z. Hashin, Failure criteria for unidirectional fiber composites, J. Appl. Mech. 47 (2015) 329–334.
[23] S.G. Zhou, C.T. Sun, Failure analysis of composite laminates with free edge, J. Compos. Technol. Res. 12 (1990) 91–97.
[24] W. Tan, B.G. Falzon, Modelling the crush behaviour of thermoplastic composites, Compos. Sci. Technol. 134 (2016) 57–71.
[25] A. Faggiani, B.G. Falzon, Predicting low-velocity impact damage on a stiffened composite panel, Compos Part A 41 (2010) 737–749.
[26] L. Liu, H. Liu, C. Kaboglu, X. Kong, Y. Ding, H. Chai, B.R.K. Blackman, A.J. Kinloch, J.P. Dear, The impact performance of woven-fabric thermoplastic and thermoset composites subjected to high-velocity soft and hard impact loading, Appl. Compos. Mater. 26 (2019) 1389–1410.
[27] H. Liu, B.G. Falzon, G. Catalanotti, W. Tan, An experimental method to determine the intralaminar fracture toughness of high-strength carbon-fibre reinforced composite aerostructures, Aeronaut. J. 122 (2018) 1352–1370.
[28] B.G. Falzon, H. Liu, W. Tan, Comment on: a tensorial based progressive damage model for fiber reinforced polymers, Compos. Struct. 176 (2017) 877–882.
[29] A. Radchenko, P. Radchenko, Numerical modeling of development of fracture in anisotropic composite materials at low-velocity loading, J. Mater. Sci. 46 (2011) 2720–2725.
[30] H. Liu, B.G. Falzon, S. Li, W. Tan, J. Liu, H. Chai, B.R.K. Blackman, J.P. Dear, Compressive failure of woven fabric reinforced thermoplastic composites with an open-hole: an experimental and numerical study, Compos. Struct. 213 (2019) 108–117.
[31] J.C. Brewer, P.A. Lagace, Quadratic stress criterion for initiation of delamination, J. Compos. Mater. 22 (1988) 1141–1196.
[32] A. Turon, C.G. Dávila, P. Camanho, J. Costa, An engineering solution for mesh size effects in the simulation of delamination using cohesive zone models, Eng. Fract. Mech. 74 (2007) 1665–1682.
[33] M.L. Benzeggagh, M. Keane, Measurement of mixed-mode delamination fracture toughness of unidirectional glass/epoxy composites with mixed-mode bending apparatus, Compos. Sci. Technol. 56 (1996) 439–449.
[34] P.P. Camanho, C.G. Davila, M.F. de Moura, Numerical simulation of mixed-mode progressive delamination in composite materials, J. Compos. Mater. 37 (2003) 1415–1437.
[35] C. Sarrado, A. Turon, J. Renart, I. Urresti, Assessment of energy dissipation during mixed-mode delamination growth using cohesive models, Compos Part A 43 (2012) 2128–2136.
[36] S. Hashemi, A.J. Kinloch, J.G. Williams, The analysis of interlaminar fracture in uniaxial fibre polymer composites, Proc. R. Soc. A427 (1990) 173–199.
[37] Overview of Materials for High Density Polyethylene (HDPE), MatWeb Material Property Data, 2018.
[38] J.E. Field, Stress waves, deformation and fracture caused by liquid impact, Philos. Trans. R. Soc. A260 (1966) 86–93.
[39] M. Lesser, Thirty years of liquid impact research: a tutorial review, Wear 186–187 (1995) 28–34.